Title

Activation of the Cpx-envelope stress response system promotes tolerance to antibacterials delivered by arginine-rich peptides and aminoglycosides in *Escherichia coli*

Authors

Jakob Frimodt-Møller[1*], Andreas Koulouktsis[1], Godefroid Charbon[1], Marit Otterlei[3], Peter E. Nielsen[2], Anders Løbner-Olesen[1*]

Affiliations

[1] Department of Biology, Center for Peptide-Based Antibiotics, University of Copenhagen, Copenhagen, Denmark.[2] Department of Cellular and Molecular Medicine, Center for Peptide-Based Antibiotics, The Panum Institute, Faculty of Health and Medical Sciences, University of Copenhagen, Copenhagen, Denmark. [3] Department of Clinical and Molecular Medicine, Faculty of Medicine and Health Sciences, NTNU, Norwegian University of Science and Technology, Trondheim, Norway.

* Corresponding authors: Jakob Frimodt-Møller (jakob.frimodtmoller@bio.ku.dk) and Anders Løbner-Olesen (lobner@bio.ku.dk).

Abstract

Cell penetrating peptides (CPP) are increasingly used for cellular drug delivery in both pro- and eukaryotic cells, and oligoarginines have attracted special attention. However; their mechanism of action, particularly for prokaryotes is still unknown. Arginine-rich CPPs (R-CPP) efficiently delivers the antimicrobial peptide nucleic acid (PNA) into bacteria. Here, we show that resistance to an R-CPP PNA conjugate in *Escherichia coli* requires multiple genetic modifications and is specific to R-CPP and not to the PNA-part. An integral part of the resistance was the constitutively activated Cpx-envelope stress response system (*cpx**), which decreased the cytoplasmic membrane potential and thereby indicates an indirectly energy dependent uptake mechanism. Interestingly, *cpx** mutants also showed increased tolerance to aminoglycosides and R-CPP conjugated to a peptide targeting the DNA sliding clamp; i.e., similar uptake in *E. coli* for these antimicrobial compounds. We speculate that the *cpx** phenotype could create an evolutionary opportunity to adapt and evolve in the presence of either compounds.

Author summary

The emergence of multidrug resistant bacteria is raising the need for new classes of antibiotics. Peptide nucleic acids (PNAs) may fill this requirement by their ability to block translation of essential mRNAs and hence inhibit growth. PNA needs conjugation to a delivery peptide (cell penetrating peptide; CPP) to enter the bacteria. Arginine-rich CPPs (CPP_R) are receiving a lot of attention for use as delivery vessels. Here, we show, for the first time, CPP_R-PNA resistance in *Escherichia coli* directed towards the delivery peptide. Consequently, resistance also applies to other antimicrobial compounds delivered by the same carrier. An

integral part of CPP_R resistance is due to a constitutive active Cpx-response system, which leads to a decreased electric potential ($\Delta\Psi$) across the inner membrane. The decreased $\Delta\Psi$ is a result of down-regulation of two aerobic respiratory operons, namely NADH:ubiquinone oxidoreductase complex I and cytochrome bo_3 ubiquinol oxidase. The decreased $\Delta\Psi$ also led to increased tolerance to aminoglycosides. This shows that a (large) negative $\Delta\Psi$ is important for providing sufficient free energy for membrane translocation of both CPP_R and that the inner membrane is the main barrier for entry of both arginine-rich delivery peptides and aminoglycosides.

Introduction

Antimicrobial resistance is one of the major challenges of the 21st century. Thus, efforts to bring novel antimicrobial compounds, including antimicrobial peptides (AMP), into clinical use are accelerating. Antisense technology, as a gene targeted precision drug modality has recently produced several new drugs in clinical use (Inotersen, Valonesorsen and Golodirsen), and agents based on the pseudopeptide DNA mimic, peptide nucleic acid (PNA)(1) and phosphorodiamidate morpholino oligonucleotide (PMO)(2) have been proposed as a future antibiotic. Naked PNA and PMO, like many AMPs, are unable to traverse the cell envelope in *Escherichia coli*(2, 3). Hence, these requires a carrier molecule (i.e., cell-penetrating peptide (CPP)) for efficient translocation into the cytoplasm. Very little is known about how CPP conjugated to PNA/PMO/AMP enters the cell and for CPP-PNA only one paper has addressed this topic(4). Here, PNA is designed to target the translation initiation region of the mRNA of an essential gene causing steric hindrance of ribosome binding, and thereby inhibition of gene expression and cell death(1). PNA conjugated to the lysine-rich CPP *L*((KFF)$_3$K) (CPP_{KFF}-PNA) enters *E. coli* by the non-essential, inner membrane transporter SbmA(4); consequently SbmA deficient *E. coli* are highly resistant to this peptide-PNA. However, PNA conjugated to an arginine-rich CPP, (R-Ahx-R)$_4$-Ahx-(βAla)-PNA (CPP_{RXR}-PNA) enters the cell in an unknown and SbmA-independent manner(4). Cationic arginine-rich CPPs (R-CPP) are increasingly used as molecular carriers and several CPP-based drugs are currently being pursued in drug discovery in relation to for example wound healing, cancer, and Duchenne Muscular Dystrophy(5). How R-CPP enters eukaryotic and prokaryotic cells is poorly understood. In eukaryotes, evidence supports predominantly an endocytotic (energy-dependent) pathway, although direct translocation (energy-independent mechanism) may also play a role (5), while it is unclear how R-CPPs penetrate through membrane lipids in prokaryotes.

The envelope of Gram-negative bacteria consists of three essential structurally and chemically diverse layers: 1) the inner membrane (cytoplasmic membrane); 2) the periplasm containing a thin peptidoglycan layer; and 3) the outer membrane that contains phospholipids in the inner leaflet and lipopolysaccharide (LPS) in the outer leaflet. *E. coli* can actively transport compounds across the cytoplasmic membrane using either ATP directly via membrane transporter proteins or indirectly via the membrane potential (partly created by the chemical proton gradient, and also being part of theproton motive force (PMF), generated by the electron transport chain). The energetics of the cell varies considerably between growth with or without oxygen, with oxidative growth conditions providing the highest energy turnover. For instance, PMF is decreased during anoxic growth conditions. The electron transport chain will under aerobic conditions predominantly contain NADH:ubiquinone oxidoreductase complex I (organized from the *nuoABCEFGHIJKLMN*-operon; NDH-I) and cytochrome bo_3 ubiquinol oxidase (organized from the *cyoABCDE* operon; cytochrome bo_3 oxidase)(6). PMF generated by translocating protons from the cytoplasm into the periplasmic space(6), serves as energy storage, which is used to drive ex. ATP synthase, efflux pumps, and transport of metabolites(7). ATP is generated from ADP and inorganic phosphate by the multi-subunit protein complex F_1F_0-ATPase(8). F_1F_0-ATPase consist of two structural domains; F_1 containing the catalytic core and F_0 containing the membrane proton channel(8). The PMF across the cytoplasmic membrane is a combination of the electric potential ($\Delta\Psi$) and the transmembrane proton gradient (ΔpH: internal pH – external pH). $\Delta\Psi$ is always negative inside growing neutrophils, such as *E. coli*, and $\Delta\Psi$ decreases as ΔpH increases(9); i.e. bacteria may regulate $\Delta\Psi$ and/or ΔpH in order to control PMF.

The Bae, Cpx, Psp, Rcs, and σ^E pathways constitute the *E. coli* signaling systems that detect and respond to alterations of the bacterial envelope(10). These pathways are involved in the biogenesis, maintenance, and repair of the bacterial envelope, and thus contribute to cell surface integrity(10). One of the most well studied extracytoplasmic stress response-systems is the CpxA/R two-component signal transduction system, which among other genes down-regulate respiratory operons when activated(11). Like many other histidine kinases, CpxA is localized to the cytoplasmic membrane through two transmembrane helices and contains both periplasmic and cytoplasmic domains(12). The cytoplasmic response regulator, *cpxR*, is predicted to encode an OmpR-like transcriptional activator(12). CpxR consist of an N-terminal receiver domain (phospho-acceptor domain) and C-terminal DNA-binding domain(13). Under non-stress conditions the

104 auxiliary regulator CpxP inhibits the Cpx-response by a predicted direct interaction with the
105 periplasmic domain of CpxA(14). Under Cpx-inducing conditions, CpxP is degraded by the
106 periplasmic protease and chaperone DegP(15). The CpxP relieved CpxA autophosphorylates on a
107 conserved histidine residue (His-248), using ATP as its phosphoryl donor(16). Subsequently,
108 phosphorylated CpxA donates its phosphoryl group to the conserved aspartate residue (Asp-51)
109 in the N-terminal receiver domain of CpxR. Phosphorylated CpxR binds to DNA and act as a
110 transcriptional regulator(16). In addition, CpxA dephosphorylates CpxR-P, which ensures that
111 CpxR remains inactive in the absence of an activating signal(17). The outer membrane lipoprotein
112 NlpE that sense surface adhesion, acts as a 'sentry protein' against envelope stress and activates
113 the Cpx-response system through an undefined interaction with CpxA(17).

114 Here we show that *E. coli* can develop tolerance to antisense PNA conjugated to R-CPPs through
115 a constitutive Cpx-response that result in a decreased $\Delta\Psi$ across the cytoplasmic membrane.
116 The decreased $\Delta\Psi$ also confers cross-resistance to aminoglycosides indicating a similar uptake
117 mechanism for the two classes of compounds.

Results

To understand bacterial uptake and resistance to PNA R-CPP conjugates, we studied the widely used CPP_{RXR}(4) (Table 1). Unless stated otherwise the PNA part always targets translation of the *acpP* mRNA, encoding the acyl carrier protein, which is essential for fatty acid synthesis(4). The CPP_{RXR}-PNA exhibited a minimum inhibitory concentration (MIC) of 0.5 µM towards *E. coli*, whereas the corresponding CPP_{RXR}-PNA containing two mismatches in the PNA sequence (PNA_{mm}) did not inhibit bacterial growth up to 16 µM (Table 1); *i.e.*, the CPP_{RXR} part alone did not confer any antimicrobial effect supporting an antisense mechanism of action. As a previous study failed to identify single-gene deletion mutants of *E. coli* resistant to CPP_{RXR}-PNA(4), we used adaptive laboratory evolution (ALE; see Methods) to generate CPP_{RXR}-PNA resistant mutants. Wild-type cells were grown in successively increasing concentrations of CPP_{RXR}-PNA, to select for mutation(s) that accumulate during long-term exposure to CPP_{RXR}-PNA. The ALE experiments were done in a biological duplicate (two independent linages) and was terminated when resistant clones appeared after 20 successive passages, corresponding to a 16-fold increase in MIC (from 0.5 µM to 8 µM) for CPP_{RXR}-PNA (Table 1).

Five individual clones from each experiment at day 20 (ten clones in total) were isolated and sequenced (Table 2; Table S1; Table S2). From the ten CPP_{RXR}-PNA resistant clones we identified three different genotypes, which were annotated as such: Ahx^R-1 to 3. Ahx^R-1 and 2 were isolated from lineage one and Ahx^R-3 from lineage two. None of the mutations identified in the CPP_{RXR}-PNA resistant clones resulted from adaptation to the growth medium, as none of them occurred in wild-type cells adapted to the same growth medium without CPP_{RXR}-PNA (Table S3).

Linage two from the ALE-experiment appeared to be clonal. This lineage contained genes/operons that were mutated in all of Ahx^R-1 to 3; the *gltF-yhcA* intergenic region, *waaB, waaO,* and *rpsL*, as well as a mutation in *cpxR* specific to only Ahx^R-3 (Table 2). *gltF* belongs to the *gltBDF*-operon, where *gltB* and *gltD* encode the large and small subunit of glutamate synthase(18), respectively. The function of GltF and the hypothetical protein YhcA, is unknown. The *waa*-operon contains the major core-oligosaccharide assembly operons in *E. coli(19)*. RpsL is the only mutated gene that is essential. The product of *rpsL* is the S12 protein; a component of the 30S subunit of the ribosome where it plays a role in translational accuracy(20). Lastly, *cpxAR* encodes the two-component regulatory system CpxA/R(21) (see above).

149 **Resistance to CPP_{RXR}-PNA is towards the arginine-rich CPP-part and not to PNA-part**

150 The MIC were determined for Ahx^R-1-3 (collectively CPP_{RXR}-PNA^R) towards additional peptide-PNA
151 conjugates (Table 1). R-PNA^R strains were also resistant to the analogous CPP_{RXR} targeting the
152 essential division protein *ftsZ* instead of *acpP*: CPP_{RXR}-PNA_{ftsZ} (Table 1). On the contrary, all R-PNA^R
153 strains remained sensitive to an *acpP* targeting PNA conjugated to the lysine-phenylalanine CPP,
154 $(KFF)_3K$ (CPP_{KFF}-PNA) (Table 1). Together this shows that resistance to CPP_{RXR}-PNA is not directed
155 towards the PNA-part but towards the (arginine-rich) delivery peptide, supporting the notion of
156 different uptake mechanism for conjugates with these two peptides.

157

158 **An activated Cpx-response leads to R-CPP tolerance**

159 The Cpx-system is known to be involved in extracytoplasmic stress response and was mutated in
160 five out of ten sequenced CPP_{RXR}-PNA resistance clones. Thus, we proceed to investigate the role
161 of the Cpx-response in tolerance to R-CPP. The highest tolerance level to CPP_{RXR}-PNA was 8 µM
162 (i.e. CPP_{RXR}-PNA^R level), which we define as CPP_{RXR}-PNA resistance. Therefore, everything between
163 wild-type CPP_{RXR}-PNA sensitivity (>0.5 µM) and CPP_{RXR}-PNA resistance is referred to as CPP_{RXR}-PNA
164 tolerance.

165 Loss of the Cpx-response, by deletion of *cpxA* or *cpxR* in otherwise wild-type cells had no effect
166 on the tolerance to CPP_{RXR}-PNA (Fig. 1A). Interestingly, increased levels of CpxR led to a small but
167 reproducible increase in tolerance to CPP_{RXR}-PNA (Fig. 1A), which could indicate that Cpx
168 activation promotes tolerance to CPP_{RXR}-PNA. We proceeded to introduce the $cpxR_{L20Q}$ mutation
169 identified in the ALE experiment (Table 2) into wild-type cells and included a $cpxA_{\Delta 16\text{-}17}$ mutant
170 into this study from our strain collection (isolated in a different project). In $CpxR_{L20Q}$, leucine is
171 replaced by glutamine at position 20, which is part of a highly conserved hydrophobic core in the
172 N-terminal receiver domain shared by OmpR-family proteins(13). In $CpxA_{\Delta 16\text{-}17}$ threonine at
173 position 16 and leucine at position 17 of the first CpxA transmembrane domain are missing. Both
174 mutations increased the MIC for CPP_{RXR}-PNA from 0.5 µM to 4 µM, relative to wild-type cells (Fig.
175 1A). Thus, although more tolerant to CPP_{RXR}-PNA than wild-type cells, the $cpxR_{L20Q}$ and $cpxA_{\Delta 16\text{-}17}$
176 mutants did not reach the CPP_{RXR}-PNA resistance level of the evolved mutant Ahx^R-3. Next, the
177 Cpx-response was tested against an oligoarginine conjugate to a peptide targeting the DNA sliding
178 clamp (DnaB; β-clamp) (RWLVK-GILQWRKI-RRRRRRRRRRR ; CPP_{R11}-APIM), which has been shown

179 to inhibit bacterial growth at micromolar concentrations both *in vitro* and *in vivo*(22) (Table 1) .
180 Loss of the Cpx-response by deletion of *cpxA* in an otherwise wild-type cell had no effect on
181 tolerance to CPP_{R11}-APIM, however tolerance was reproductively increased from 1 µM to 2 µM in
182 the $cpxR_{L20Q}$ and $cpxA_{\Delta 16\text{-}17}$ mutants, relative to wild-type cells (Fig. 1B). Thus this peptide also
183 exhibits tolerance to the Cpx-mutants but only at a 2 fold increase compared to 8 fold for the
184 CPP_{RXR}-PNA.

185 We used *cpxP* transcription as a readout for activation of the *cpx* response(23). $cpxR_{L20Q}$, $cpxA_{\Delta 16\text{-}}$
186 $_{17}$, and Ahx^{R}-3 all had increased expression of *cpxP* compared to wild-type (Fig. 1C), albeit not to
187 the level achieved by overproduction of NlpE (full activation of the Cpx-response; Fig. 1C). This
188 confirmed that the Cpx-response was indeed activated by the $cpxR_{L20Q}$ and $cpxA_{\Delta 16\text{-}17}$ mutations
189 and that these provided CPP_{RXR}-PNA (and CPP_{R11}-APIM tolerance) to the same level as full
190 activation of the Cpx-response by NlpE overproduction (Fig. 1B, D). Both mutations are therefore
191 gain-of-function mutations leading to a constitutively active Cpx-response, which previously have
192 been denoted *cpx**(16, 17).

193

194 **Both $cpxR_{L20Q}$ and $cpxA_{\Delta 16\text{-}17}$ mutations are dependent on a functional Cpx-system for conferring**
195 **CPP_{RXR}-PNA tolerance**

196 To assess whether the $cpxA_{\Delta 16\text{-}17}$ and $cpxR_{L20Q}$ mutations were dependent on a functional Cpx
197 system for conferring CPP_{RXR}-PNA tolerance, *cpxA* was deleted in the $cpxR_{L20Q}$ strain and *cpxR* was
198 deleted in the $cpxA_{\Delta 16\text{-}17}$ strain. In either case, CPP_{RXR}-PNA tolerance was reduced to wild-type
199 level (Fig. 1A). Thus, the substitution to glutamine in position 20 in CpxR does not make it
200 constitutively active by mimicking phosphorylation of the conserved Asp-51, and $CpxR_{L20Q}$ still
201 relies on a functional CpxA to be activated. Overproduction of wild-type CpxR or CpxA in the
202 $cpxR_{L20Q}$ or $cpxA_{\Delta 16\text{-}17}$ mutants, respectively, also restored CPP_{RXR}-PNA susceptibility to wild-type
203 level (Fig. 1A). Together, this shows that the specific $cpxR_{L20Q}$ or $cpxA_{\Delta 16\text{-}17}$ mutations mediates
204 CPP_{RXR}-PNA tolerance, but do need a functional Cpx-system.

205

206 **The Cpx-response is the only extracytoplasmic stress response conferring tolerance to CPP_{RXR}-**
207 **PNA**

208 The Cpx-response is only one of five extracytoplasmic stress response systems known to maintain
209 cell envelope integrity during stress. While the Cpx-response can be activated by overproducing
210 *nlpE,* the four other extracytoplasmic stress responses can be individually activated by
211 overproduction of *baeR* for the Bae-pathway, *rcsB* for the Rcs-pathway, *pspF* for the Psp-pathway,
212 and *rpoE* for the σ^E-pathway(10). Activation of neither the Bae, Psp, Rcs, nor the σ^E-responses led
213 to a CPP_{RXR}-PNA tolerant phenotype (Fig. 1D), showing CPP_{RXR}-PNA tolerance is specific to an
214 activated Cpx-response. However, wild-type treated with sub-MIC concentrations (0.5 X MIC) of
215 CPP_{RXR}-PNA or CPP_{RXR}-PNA_{mm} did not result in an increased *cpxP* expression (Fig. 1D). Hence,
216 although an activated Cpx-response confers CPP_{RXR}-PNA tolerance, low-level CPP_{RXR}-PNA
217 treatment in itself does not trigger extracytoplasmic stress.

218

219 **Downregulation of respiratory operons leads to CPP_{RXR}-PNA tolerance**

220 Because Cpx mediates downregulation of aerobic respiratory operons(11), expression of the
221 *nuoABCEFGHIJKLMN* and *cyoABCDE* operons were determined by RT-qPCR. As expected,
222 transcription of *nuoA* (to evaluate expression of the *nuoABCEFGHIJKLMN* operon) and *cyoA* (to
223 evaluate expression of the *cyoABCDE* operon) were downregulated in wild-type/pCA24n:*nlpE*,
224 $cpxR_{L20Q}$, $cpxA_{\Delta 16\text{-}17}$, and Ahx^R-3 cells (Fig. 2A). We found that such Cpx activated cells in addition
225 to being CPP_{R11}-APIM ($cpxR_{L20Q}$ and $cpxA_{\Delta 16\text{-}}$17; Fig. 2B) and CPP_{RXR}-PNA tolerant (Fig. 2B) were also
226 more tolerant to the aminoglycosides gentamicin, amikacin, and kanamycin (Fig. 2C) than the
227 wild-type. When the entire *nuoABCEFGHIJKLMN* and *cyoABCDE* operon were individually deleted
228 from wild-type cells, the resultant Δ*nuo* and Δ*cyo* strains were more tolerant to both CPP_{R11}-APIM
229 (only tested with Δ*cyo*), CPP_{RXR}-PNA and aminoglycosides relative to the wild-type (Fig. 2B,C). This
230 confirms that CPP_{R11}-APIM, CPP_{RXR}-PNA, and aminoglycoside tolerance in $cpxR_{L20Q}$ and $cpxA_{\Delta 16\text{-}17}$
231 is related to aerobic oxidative phosphorylation and result from downregulation of NDH-I and
232 cytochrome bo_3 oxidase.

233

234 **The cytoplasmic membrane potential (ΔΨ) directly affects CPP_{RXR}-PNA and CPP_{R11}-APIM activity**

235 Downregulation of respiratory operons suggested that the ΔΨ formed across the inner membrane
236 plays a significant role in CPP_{R11}-APIM CPP_{RXR}-PNA tolerance. We determined the ΔΨ at the
237 intracellular pH 7.6 of *E. coli* based on the distribution of the lipophilic tetraphenylphosphonium

238 ion (TPP^+) using a TPP^+-selective electrode(24). At this pH value the Δ*pH* is zero and the PMF is
239 only dependent on ΔΨ. Wild-type cells had a ΔΨ of approx. -140 mV, in accordance with previous
240 observations(25) (Fig. 2D). The ΔΨ was reduced by the $cpxR_{L20Q}$ as well as the $cpxA_{\Delta 16\text{-}17}$ mutation
241 (Fig. 2D). Δ*cyo* and Δ*nuo* cells also had a decreased ΔΨ compared to wild-type; with values
242 comparable to $cpxR_{L20Q}$ and $cpxA_{\Delta 16\text{-}17}$ (Fig. 2D). Thus, it is conceivable that the decreased ΔΨ of
243 $cpxR_{L20Q}$ and $cpxA_{\Delta 16\text{-}17}$ cells may result from downregulation of the respiratory operons.

244

245 *E. coli* maintains a stable PMF across the inner membrane, such that ΔΨ decreases with an
246 increase in Δ*pH* in an acidic medium, vice versa in an alkaline media (9) (Fig. 3). Thus, ΔΨ can be
247 modulated by growing the cells at various pH levels. In acidic media (pH 6.0) where ΔΨ is
248 decreased(9) (Fig. 3A), wild-type cells were tolerant to CPP_{RXR}-PNA, CPP_{R11}-APIM and gentamicin
249 (Fig. 3A), while an increased ΔΨ due to growth in alkaline media (pH 8.0)(9) resulted in sensitivity
250 to both CPP_{RXR}-PNA, CPP_{R11}-APIM and gentamicin (Fig. 3B). The changes in ΔΨ in the two different
251 pH-adjusted settings had no effect on tolerance to CPP_{KFF}-PNA (Fig. 3A,B). *E. coli* cells deficient of
252 the F_1F_0-ATPase or supplemented with alanine have been shown to have an increase in ΔΨ(26,
253 27) and were more sensitive to CPP_{RXR}-PNA, gentamicin, and CPP_{R11}-APIM (only tested with
254 alanine), but sensitivity to CPP_{KFF}-PNA was similar to wild-type (Fig. 3B). Finally, ΔΨ is decreased
255 under anaerobic growth conditions(26) explaining why wild-type under these conditions are more
256 tolerant to CPP_{RXR}-PNA and gentamicin (Fig. 3A). Most likely the effect of ΔΨ on antimicrobial
257 activity is explained by increased inner membrane passage of the polycationic molecules
258 energetically driven by the negative membrane potential.

259

260 **Neither $cpxR_{L20Q}$ nor the $cpxA_{\Delta 16\text{-}17}$ mutations conferred resistance to cationic antimicrobial**
261 **peptides**

262 Cationic antimicrobial peptides represent the biggest class of antimicrobial peptides and the
263 majority of these are amphipathic. Here, Cap11, Cap18, cecropin P1, apidaecin 1B, indolicidin,
264 protamine, and the most well-known polypeptide antibiotic colistin were tested against wild-type,
265 $cpxR_{L20Q}$, $cpxA_{\Delta 16\text{-}17}$, and Ahx^R-3 (Table S4). Colistin, Cap11, Cap18, protamine, and cecropin P1 are
266 believed to target the cell envelope (disruption of bilayers), while indolicidin (disruption of bilayers
267 and DNA synthesis) and apideacin 1B (ribosomes) have intracellular targets. An activated Cpx-

268 response and a decrease in $\Delta\Psi$ did not confer tolerance to any of the tested AMPs (Table S4).
269 Interestingly, the evolved strain Ahx^R-3 was more susceptible to Cecropin P1, Cap11, Cap18, and
270 colistin than wild-type (Table S4). One of the major differences between wild-type and Ahx^R-3 is
271 the two IS1-insertions in *waaB* and *waaO* in Ahx^R-3 (Table 2). This is expected to result in LPS
272 deficiency, which is associated with an increased susceptibility to cationic antimicrobial peptides
273 in *E. coli*(28). Accordingly, when *waaBO* were deleted in the wild-type (Δ*waaBO*) they became
274 more susceptible to Cecropin P1, Cap11, Cap18, and colistin but not to CPP_{R11}-APIM.

275

276 **High CPP_{RXR}-PNA tolerance is associated with fitness cost**

277 The doubling times of $cpxR_{L20Q}$ and $cpxA_{\Delta 16\text{-}17}$ mutants were 28 min and 27 min, respectively, when
278 grown aerobically in MHB I at 37°C and somewhat slower than that of wild-type cells (25 min).
279 The reduced doubling times are likely to result from repression of the respiratory operons in the
280 respective mutants. Of interest, the evolved mutant, Ahx^R-3 (58 min), which conferred the highest
281 resistance to R-PNA (8 µM vs. 4 µM for the $cpxR_{L20Q}$ and $cpxA_{\Delta 16\text{-}17}$ mutants), grew more than twice
282 as slow as both the wild-type and the $cpxR_{L20Q}$ and $cpxA_{\Delta 16\text{-}17}$ mutants. This shows that CPP_{RXR}-PNA
283 resistance comes with a high fitness cost.

Discussion

Since the late eighties, natural and synthetic CPPs have been developed and modified for applications in both basic- and applied biology including delivery of therapeutic agents, gene editing and cell imaging. Due to efficient delivery, CPPs as carriers for therapeutic compounds to treat various diseases has gained attraction in recent years(5). Although there are many types of CPPs with different physicochemical properties and applications, R-CPPs, are among the most extensively employed and studied(29). PNA, PMO and AMPs are novel, promising antimicrobial agents, of which PNA and PMO require conjugation to a CPP for delivery to the intracellular targets in bacteria(4). Here, we isolated and characterize resistant strains towards an R-CPP. High-level resistance to the arginine-rich CPP-part was difficult to obtain, came with a high fitness cost, and it conferred cross-resistance to aminoglycosides, which is seen as a clear disadvantage for the use of these carriers in antibacterial therapy.

The cytoplasmic membrane is the main barrier for CPP_{RXR}-PNA

The initial interaction with the envelope differs between CPP_{R11}-APIM/CPP_{RXR}-PNA and cationic AMPs. Thus, loss of LPS had no effect on the activity of CPP_{RXR}-PNA or CPP_{R11}-APIM while this sensitized wild-type to the cationic AMPs (Table S4). It therefore remains unclear why LPS deficiency were selected in Ahx^R-1, 2, and 3. A reduction of $\Delta\Psi$ in the cytoplasmic membrane was found to diminish/reduce CPP_{RXR}-PNA and CPP_{R11}-APIM activity, demonstrating that a (large) negative $\Delta\Psi$ is important for activity, and most likely for providing sufficient free energy required for membrane translocation. The more detailed mechanism of membrane passage is not known, but could rely on direct, local membrane interruption or be aided by one or more still unidentified transporter protein. However, for CPP_{RXR}-PNA neither our ALE study nor a previous screening of the KEIO collection(4) provides evidence for the existence of a single CPP_{RXR}-PNA transport mechanism. However, we cannot exclude that CPP_{RXR}-PNA is the substrate of multiple transport systems, in which case the absence of one would be compensated by the remaining other(s).

CPP_{RXR}-PNA resistance arise in multiple steps

Several genetically different R-PNA^R mutants arose both within and across the two lineages in the ALE-experiment. This suggest clonal interference within the populations of each ALE lineage,

where mutants will compete not just against the susceptible parent but also against each other(30). Clonal interference influences evolutionary trajectories, which typically leads to a population with one dominant clone(31), as suggested here for clone Ahx^R-3. The evolutionary paths leading to three genotypes, from the two linages, speaks to either multiple ways to become CPP$_{RXR}$-PNA resistance or that they all, more or less, confer the same universal CPP$_{RXR}$-PNA^R phenotype. Nonetheless, resistance development to PNA conjugated to an R-CPP is complex, requiring multiple mutations in independent loci to create the CPP$_{RXR}$-PNA^R phenotype (Table 2). This is in stark contrast to the straightforward resistance development to PNA conjugated to the lysine-rich CPP, i.e. CPP$_{KFF}$-PNA, by a loss-of-function mutation in the *E. coli sbmA* gene(4). We show that the *cpx**-phenotype is a major part of the CPP$_{RXR}$-PNA resistance phenotype in Ahx^R-3, but that additional mutations are required for high-level resistance. As observed for *waaBO*, not all mutations from the ALE-experiment on their own resulted in CPP$_{RXR}$-PNA tolerance. Either, the *waaBO* mutation requires another mutation to synergistically provide CPP$_{RXR}$-PNA tolerance or it was selected as a mutation that compensate a fitness cost associated with mutations conferring CPP$_{RXR}$-PNA resistance. Indeed, CPP$_{RXR}$-PNA^R strains have increased doubling time, highlighting that CPP$_{RXR}$-PNA resistance comes with a cost.

The cpx phenotype relies on a functional Cpx-system*

Our results show that alterations in the first transmembrane domain of CpxA can produce a *cpx** phenotype. Several gain-of-function mutations in *cpxA* have been reported(16, 17), but most cluster to and around the second transmembrane domain of CpxA(17). We suggest that the deletion in the first transmembrane domain leads to a conformational change in the periplasmic part of CpxA, which either disallows CpxP regulation or simulates the stress signal that actives the Cpx-response; i.e. a constitutive active CpxA. To the best of our knowledge, *cpxR$_{L20Q}$* is the first reported mutation in *cpxR* resulting in a *cpx** phenotype. The activated Cpx-response in the *cpxR$_{L20Q}$* mutant was CpxA-dependent; i.e. the *cpxR$_{L20Q}$* mutation does not result in a constitutive phosphorylated CpxR. Therefore, it is likely that the *cpxR$_{L20Q}$* mutation inhibits/diminish the ability of CpxA to dephosphorylate CpxR-P to CpxR, which in turn results in a constitutive active Cpx-response. CpxA and CpxR-P both function as dimers(32). Thus overproducing the respective wild-type allele in the two mutants restored sensitivity to CPP$_{RXR}$-PNA by either hetero-dimerization of a mutated and a wild-type protein, with the wild-type being dominant to the mutant, or by homo-

dimerization of either mutated or wild-type proteins, but with wild-type dimer domination due to abundance.

Low cytoplasmic membrane potential correlates with tolerance to CPP_{RXR}-PNA, CPP_{R11}-APIM, and aminoglycosides

We found that a reduction of the $\Delta\Psi$ component of PMF across the cytoplasmic membrane increased tolerance to both CPP_{RXR}-PNA, CPP_{R11}-APIM, and aminoglycosides; the latter in agreement with previous studies in *Bacillus subtilis* and *E. coli*(33). The reduced activity of both CPP_{RXR}-PNA, CPP_{R11}-APIM, and aminoglycosides when $\Delta\Psi$ was decreased indicates that crossing of the inner (and not the outer) membrane is the rate limiting and energy dependent step shared by this type of (polycationic) compounds as previously proposed for aminoglycosides (34). Once inside the bacterial cells, aminoglycosides interacts with the 30S subunit of ribosomes, RXR-PNA prevent *acpP* translation, and CPP_{R11}-APIM prevent β-clamp function (Fig. 4A). In wild-type cells, CPP_{RXR}-PNA (and possibly also aminoglycosides and, CPP_{R11}-APIM) do not activate the Cpx-response. We propose that *cpx** dependent tolerance to CPP_{RXR}-PNA, CPP_{R11}-APIM, and aminoglycosides is caused by downregulation of respiratory complexes in the cytoplasmic membrane (Fig. 4B) thereby decreasing $\Delta\Psi$ across the cytoplasmic membrane at least partly due to the reduced ATP level and consequently reduced proton chemical potential over the membrane, making it less energetically favorable for R-CPP to transvers the cytoplasmic membrane (Fig. 4B). CPP_{KFF}-PNA is internalized in a SbmA-dependent manner(4) (for which a membrane potential driving force apparently is not important) and therefore the CPP_{RXR}-PNA^{R} strains were sensitive to CPP_{KFF}-PNA.

The cpx phenotype could lead to the acquisition of other mutations to promote resistance or persistance*

The *cpx** phenotype provides moderate resistance to both CPP_{RXR}-PNA and aminoglycosides – all without a major loss of fitness. Thus, in a clinical setting, *cpx** mutants could grow in the presence of moderate levels of either compound, which in turn would create an evolutionary opportunity to adapt and evolve by subsequent acquisition of mutations to further increase resistance or to assist in persistent colonization. Several recent studies have shown that adaptation, may have a

375 significant impact on the selection of highly resistant/persistent clones for *Mycobacterium*
376 (ribosomal mutations)(35), *Pseudomonas aeruginosa* (efflux pump regulator mutation)(36), and
377 *E. coli* (formation of subpopulations with an increased overall mutation rate)(37). Thus, the *cpx**
378 phenotype may be added to this list.

Materials and Methods

Growth conditions

Cells were grown in Luria–Bertani Broth (LB) medium or Müller-Hinton I Broth (MHBI) at 37°C with aeration unless stated otherwise. When necessary, antibiotics were added to the following concentrations: chloramphenicol, 20 µg/mL; ampicillin, 150 µg/mL; kanamycin, 50 µg/mL; tetracyclin, 10 µg/mL.

Peptide conjugates

PNA-peptide conjugates were synthezised as described previously (1, 4). CPP_{R11}-APIM (RWLVK* with the complete sequence Ac-MD-RWLVK-GILQWRKI-RRRRRRRRRRR) is described previously(22).

Bacterial strains and plasmids

A MG1655 strains used in this study are listed in Table S5 and all primer sequences in Table S6. For deleting and overexpressing genes, we used the KEIO collection(38) and the ASKA library(39), respectively. Shortly, the *cpxA, cpxR, degP,* or *cpxP* deletion/replacement mutations were obtained from the KEIO collection(38) and P1 transduced(40) into *E. coli* MG1655 to create ALO6524, ALO6525, ALO7548, and ALO7549, respectively. For overexpression of genes, pCA24n based plasmids from the ASKA collection was transformed into *E. coli* MG1655 selecting for chloramphenicol.

Deletion of the *nuoABCEFGHIJKLMN, cyoABCDE,* and *waaBO* chromosomal regions in wild-type was constructed by the lambda red procedure(41). Briefly, primer sequences were obtained from Baba *et al.* (38) and are listed in Suppl. Table 2. The *nuo*_cat_Fw primer corresponds to the 5′ primer used to delete *nuoA* in Baba *et al.* (38), while the *nuo*_cat_Rv primer corresponds to the 3′ primer used to delete *nuoN* in Baba *et al.* (38). The *cyo*_cat_Fw primer corresponds to the 5′ primer used to delete *cyoA* in Baba *et al.* (38), while the *cyo*_cat_Rv primer corresponds to the 3′ primer used to delete *cyoE* in Baba *et al.* (38). The *waaB*_cat_Fw primer corresponds to the 5′ primer used to delete *waaB* in Baba *et al.* (38), while the *waaO*_cat_Rv primer corresponds to the 3′ primer used to delete *waaO* in Baba *et al.* (38). DNA fragments were PCR amplified using the

408 primer sets *nuo*_cat_Fw + *nuo*_cat_Rv, *cyo*_cat_Fw + *cyo*_cat_Rv, and *waaB*_cat_Fw +
409 *waaO*_cat_Rv to delete *nuoABCEFGHIJKLMN, cyoABCDE,* and *waaBO,* respectively. PCR
410 amplification was done using high-fidelity Phusion DNA polymerase (Thermo Scientific™)
411 according to the manufacturer's specifications with pKD3 as template. The resultant DNA
412 fragments were introduced into wild-type cells bearing pKD46(41), selecting for chloramphenicol
413 resistance. Each deletion was verified by PCR creating Δ*nuoABCEFGHIJKLMN* (Δ*nuo*; ALO7555),
414 Δ*cyoABCDE* (Δ*cyo*; ALO7556), and Δ*waaBO* (ALO6972).

415 The $cpxR_{L20Q}$ mutations were introduced into the wild-type using the Tet/SacB counter-selection
416 and recombineering approach(42). Briefly, the *tet-sacB* cassette flanked by appropriate homology
417 arms was amplified using the primer set CpxR_*tet-sacB*_Fw + CpxR_*tet-sacB*_Rv using pTETSACB
418 as a template for exchange of *cpxR* in the wild-type. The resultant DNA fragments were introduced
419 into wild-type bearing pKD46(41), selecting for tetracycline and ampicillin resistance at 32°C (to
420 keep pKD46 in the cell) creating *cpxR*:*tet-sacB* pKD46. The deletion was verified by PCR. Next, the
421 $CpxR_{L20Q}$ mutations were amplified from Ahx^R-3 with homology flaking the inserted *tet-sacB*
422 cassettes, using the primer sets $CpxR_{L20Q}$_Fw + $CpxR_{L20Q}$_Rv. The resultant DNA fragments
423 containing the $cpxR_{L20Q}$ mutation were introduced into *cpxR*:*tet-sacB* selecting for growth on LB
424 agar containing 6% sucrose. *cpxR* genes from clones that were tetracycline sensitive and able to
425 grow on sucrose were sequenced to confirm the introduction of the specific mutations from Ahx^R-
426 3 into wild-type, thus creating the strain $cpxR_{L20Q}$ (ALO7180). *cpxA* was deleted in $cpxR_{L20Q}$ and
427 *cpxR* was deleted in $cpxA_{\Delta 16\text{-}17}$ by P1 transduction (as above) creating $cpxR_{L20Q}$ Δ*cpxA* (ALO7550)
428 and $cpxA_{\Delta 16\text{-}17}$ Δ*cpxR* (ALO7551), respectively. In addition, *nuoABCEFGHIJKLMN* and *cyoABCDE*
429 were deleted as above in $cpxR_{L20Q}$ using the lambda red procedure(41) created $cpxR_{L20Q}$ Δ*nuo*
430 (ALO7552) and $cpxR_{L20Q}$ Δ*cyo* (ALO7553), respectively.

431

432 **Adaptive Laboratory Evolution (ALE) experiment**

433 Wild-type was evolved for 20 days to CPP_{RXR}-PNA, with two lineages evolved in parallel for each
434 drug. Here, 1 x 10^5 CFU/mL of cells were inoculated in 2-fold peptide-PNA gradient in 8 dilutions
435 in 100 µl MHBI in a 96-well polystyrene microtitre plate and grown for 18-24 hours at 37°C. The
436 following day the population grown in the highest concentration of peptide-PNA where re-diluted
437 to 1 x 10^5 CFU/mL and inoculated in a fresh 2-fold peptide-PNA gradient as above. After 20
438 successive passages, five peptide-PNA resistant single clones were isolated from each lineage and

439 whole genome sequenced. As control, *E. coli* MG1655 was evolved to the MHBI in four
440 independent biological replicates without the presence of peptide-PNA. Here, two clones were
441 isolated and whole genome sequenced for each lineage.

442

443 **Extraction of genomic DNA**

444 Genomic DNA of *E. coli* MG1655 was isolated using phenol/chloroform extraction. Shortly, cells
445 from a 15 ml culture were collected at an OD_{600} of 0.5 by centrifugation at 5.000 ×g for 10 minutes.
446 The pellet was resuspeded in 1 ml 0.9% NaCl, followed by a centrifugation at 10.000 ×g for 5
447 minutes. The cells were lysed by incubation at 37°C for 1 hour with 600 µl lysis buffer (Tris-EDTA
448 buffer (TE buffer, pH 8.0), 10% (w/v) SDS, 20 mg/ml proteinase K, 1 mg/ml RNase A). Following
449 two phenol- and two chloroform-extraction, DNA was precipitated using NaCl (0.2 M) and 0.6 vol.
450 isopropanol, washed in 80% ethanol and resuspended in TE buffer (pH 8.0).

451

452 **Whole genome sequencing and data analysis**

453 Reads were mapped to MG1655 NC_000913.3 using BWA-MEM. Variants were extracted using
454 Freebayes (only variants with >50 % frequency were retained). For location of IS insertion, mapped
455 reads with <60 mapQuality were selected and paired reads (CIGAR-Left-clip/Right-Clip, CIGAR-D
456 and CIGAR-I) were aligned to NC_000913.3 using NCBI Blast to confirm deletion /insertion.

457

458 **Antimicrobial Susceptibility Testing**

459 MIC values were determined by broth microdilution according to the standard protocol(43) with
460 a few modifications. Shorty, an overnight bacterial cell culture was diluted to approximately 5 ×
461 10^5 CFU/mL in MHBI. 100 µL bacterial solution was dispensed into a low-bind 96-well plate
462 (Thermo-Scientific, cat.no. 260895) along with 11 µL of the test compound (2-fold dilutions). The
463 plate was incubated at 37°C for 18-24 h. The MIC was determined as the lowest concentration,
464 which inhibited visible growth in the wells (OD_{595} nm < 0.1). Peptide-PNAs were dissolved in 0,02%
465 acetic acid containing 0,4% bovine serum albumine and dilution were performed in 0,01% acetic
466 acid containing 0,2% BSA, while gentamicin, amikacin, kanamycin, cecropin P1, Cap11
467 (Genescript), Cap18 (Genescript), apidaecin 1B (Genescript), colistin, indolicidin and protamine

468 (Sigma-Aldrich) was diluted according to vendors specifications. To determine MIC under acidic
469 and alkaline conditions, MHBI was buffered to pH 6.0 or pH 8.0 using citrate buffer (pH 3.0) and
470 carbonate-bicarbonate buffer (pH 10.0), respectively. Anaerobic growth for MIC determinations
471 was performed in a double sealed bag using anaerobic atmosphere generation bags (Becton,
472 Dickinson and Company, New Jersey, USA). MHBI was supplemented with 0.1 mM Isopropyl β-D-
473 1-thiogalactopyranoside (IPTG), when tested strains harbored pCA24n-based plasmids.

474

475 **Total RNA extraction**

476 RNA were isolated from cells by the hot phenol method. Shortly, cells were grown in cation
477 adjusted MHBI to mid-log phase, an OD_{595} of 0.2 (2.5×10^9 cells/ml), by shaking at 150 rpm and
478 37°C. To induce protein expression in cells harboring the inducible pCA24n-based plasmid, IPTG
479 was added to a concentration of 0.1 mM at an optical density OD_{595} 0.005. Bacteria from 2-ml
480 aliquot were harvested by centrifugation at 4°C and 17.000×g for 5 minutes. The pellets were
481 resuspended in the same volume of RNAprotect Bacteria Reagent (QIAGEN, Denmark), incubated
482 at room temperature for 5 minutes, followed by a centrifugation using the same conditions as
483 above. The supernatants were discarded and the pellets were either stored at -80°C until needed
484 or immediately used for RNA extraction.

485 To extract RNA, the pellets were lyzed in 200 µl Solution I [0.3 M sucrose, 0.01 M sodium acetate
486 (NaOAc) and pH 4.5] at 4°C and mixed thoroughly. Then, 200 µl of Solution II (2% (w/w) Sodium
487 dodecyl sulfate (SDS), 0.01 M NaOAc and pH 4.5) were added at room temperature and solutions
488 were gently mixed by inversion of tubes. Next, a volume of 400 µl of acid
489 phenol:chloroform:isoamyl alcohol 125:24:1 was added and immediately mixed (vortex) to
490 emulsify. The samples were incubated at 65°C for 10 minutes and mixed (vortex) for 5-10 seconds
491 every minute. Then, tubes were transferred on ice for 5 minutes and centrifuged at 14.000 rpm
492 for 5 minutes. The aqueous phase was transferred to a new polypropylene tube and one-fifth
493 volume of chloroform was added and gently mixed by inversion, followed by centrifugation at
494 14.000 rpm for 5 minutes. This step was repeated by addition of the same volume of
495 chloroform:isoamyl alcohol 24:1. To precipitate RNA, the aqueous phase was transferred to a new
496 tube, mixed with the same volume of isopropanol and incubated at -80°C for a minimum of 1 hour.
497 RNA was precipitated by spinning down at 4°C and 12.000 ×g for 30 minutes, followed by wash

with 1 ml 70% ethanol and centrifugation at 4ºC and 12.000 ×g for 5 minutes. The pellets were resuspended in 30 µl nuclease free water and RNA concentration and purity was determined using a NanoDrop.

Following removal of genomic DNA by DNase I (Qiagen, Venlo, Netherlands), RNA were purified using RNeasy MinElute Cleanup kit (Qiagen) and following the vendors instructions.

qRT-PCR.

For qRT-PCR experiments, after genomic DNA digestion, 1 µg of total RNA was retrotranscribed using QuantiTect Reverse Transcription kit (Qiagen). Primers designed to amplify *cpxP*, *nuoA*, and *cyoA* (Table 8) were targeted to regions of unique sequences within the genes in wild-type *E. coli* MG1655. The qRT-PCR was performed using the TB Green Premix Ex Taq II (Takara Bio Inc., Shiga, Japan) on a QuantStudio 3 Real-Time PCR System (Thermo Fisher Scientific, Massachusetts, United States). All data were normalized to the reference genes *hctA* and *cysG*. These data were transformed to log2 to obtain a change difference (n-fold) between strains.

Determination of membrane potential (Δψ) by measuring Tetraphenyl phosphonium (TTP^+) uptake using the TPP^+-selective electrode method

The membrane potential was determined by measuring the uptake of the permeating lipophilic cationic probe, Tetraphenyl phosphonium (Merck KGaA, Germany). An overnight culture was diluted (5.000-fold) in MHBI, and cells from 25 ml culture were harvested when OD_{595} reached 0.2. Cells were washed twice in 0.1 M Tris·HCl (pH 8.1) using the conditions mentioned above, and the pellets were gently resuspended in 1 ml of the same buffer. To generate cells permeable to TPP^+, after a first incubation for 6 minutes at 36ºC with occasional agitation, bacteria were treated with K^+-EDTA to a concentration of 10 mM and then incubated at 36ºC for 3 more minutes. Cells were diluted 10-fold in ice-cold 0.1 M potassium phosphate buffer (0.1 M K_2HPO_4; 0.1 M KH_2PO_4; pH 7.5), to remove EDTA, followed by immediate centrifugation in the cold at 13.000 rpm for 7 minutes. The cells were washed twice in the same ice-cold buffer using the parameters mentioned above, and the pellets were resuspended, to an OD_{595} of 20.0, in 10 mM potassium phosphate

buffer (pH 7.5) containing 200 mM NaCl, 0.14 mM $CaCl_2$, 0.1 mM $MgSO_4$ and 0.01 mM $MnCl_2$. The cells were kept on ice until use.

Bacteria were added to an OD_{595} of 4.0 in 10 ml of the same buffer supplemented with glucose and TPP^+ to a concentration of 5 mM and 10 µM, respectively, and TPP^+ uptake was measured utilizing the TPP^+-selective electrode method described by Hosoi *et al*(44). TPP^+ concentration in the external medium was determined using a Kwik-Tip™ Ag/AgCl half-cell electrode, which was constructed according to the instructions provided by the manufacturer (World Precision Instruments, Sarasota, FL). Both the TPP^+-selective electrode and a Flexible Dri-Ref reference electrode (World Precision Instruments, Sarasota, FL) were connected to an Jenway 3510 ion meter (Cole-Parmer, Staffordshire, UK) and LabTrax 4-Channel Data Acquisition system (WPI). Finally, TPP^+ uptake measurements were carried out in a 15 ml closed tube, at 30°C and pH 7.5 for 10 minutes, and data were recorded using the iWorx LabScribe recording and analysis software (iWorx Systems Inc., Dover, NH).

References and Notes

1. Good L, Nielsen PE. Antisense inhibition of gene expression in bacteria by PNA targeted to mRNA. Nat Biotechnol. 1998;16(4):355-8.
2. Wesolowski D, Tae HS, Gandotra N, Llopis P, Shen N, Altman S. Basic peptide-morpholino oligomer conjugate that is very effective in killing bacteria by gene-specific and nonspecific modes. Proc Natl Acad Sci U S A. 2011;108(40):16582-7.
3. Good L, Sandberg R, Larsson O, Nielsen PE, Wahlestedt C. Antisense PNA effects in Escherichia coli are limited by the outer-membrane LPS layer. Microbiology. 2000;146 (Pt 10):2665-70.
4. Ghosal A, Vitali A, Stach JE, Nielsen PE. Role of SbmA in the uptake of peptide nucleic acid (PNA)-peptide conjugates in E. coli. ACS Chem Biol. 2013;8(2):360-7.
5. Habault J, Poyet JL. Recent Advances in Cell Penetrating Peptide-Based Anticancer Therapies. Molecules. 2019;24(5).
6. Ingledew WJ, Poole RK. The respiratory chains of Escherichia coli. Microbiol Rev. 1984;48(3):222-71.
7. Gunner MR, Amin M, Zhu X, Lu J. Molecular mechanisms for generating transmembrane proton gradients. Biochim Biophys Acta. 2013;1827(8-9):892-913.
8. Vik SB, Antonio BJ. A mechanism of proton translocation by F1F0 ATP synthases suggested by double mutants of the a subunit. J Biol Chem. 1994;269(48):30364-9.
9. Kashket ER. The proton motive force in bacteria: a critical assessment of methods. Annu Rev Microbiol. 1985;39:219-42.
10. Bury-Mone S, Nomane Y, Reymond N, Barbet R, Jacquet E, Imbeaud S, et al. Global analysis of extracytoplasmic stress signaling in Escherichia coli. PLoS Genet. 2009;5(9):e1000651.
11. Raivio TL, Leblanc SK, Price NL. The Escherichia coli Cpx envelope stress response regulates genes of diverse function that impact antibiotic resistance and membrane integrity. J Bacteriol. 2013;195(12):2755-67.
12. Weber RF, Silverman PM. The cpx proteins of Escherichia coli K12. Structure of the cpxA polypeptide as an inner membrane component. J Mol Biol. 1988;203(2):467-78.
13. Itou H, Tanaka I. The OmpR-family of proteins: insight into the tertiary structure and functions of two-component regulator proteins. J Biochem. 2001;129(3):343-50.
14. Raivio TL, Popkin DL, Silhavy TJ. The Cpx envelope stress response is controlled by amplification and feedback inhibition. J Bacteriol. 1999;181(17):5263-72.
15. Buelow DR, Raivio TL. Cpx signal transduction is influenced by a conserved N-terminal domain in the novel inhibitor CpxP and the periplasmic protease DegP. J Bacteriol. 2005;187(19):6622-30.
16. Danese PN, Snyder WB, Cosma CL, Davis LJ, Silhavy TJ. The Cpx two-component signal transduction pathway of Escherichia coli regulates transcription of the gene specifying the stress-inducible periplasmic protease, DegP. Genes Dev. 1995;9(4):387-98.
17. Raivio TL, Silhavy TJ. Transduction of envelope stress in Escherichia coli by the Cpx two-component system. J Bacteriol. 1997;179(24):7724-33.
18. Castano I, Bastarrachea F, Covarrubias AA. gltBDF operon of Escherichia coli. J Bacteriol. 1988;170(2):821-7.
19. Raetz CR, Dowhan W. Biosynthesis and function of phospholipids in Escherichia coli. J Biol Chem. 1990;265(3):1235-8.
20. Alksne LE, Anthony RA, Liebman SW, Warner JR. An accuracy center in the ribosome conserved over 2 billion years. Proc Natl Acad Sci U S A. 1993;90(20):9538-41.
21. Otto K, Silhavy TJ. Surface sensing and adhesion of Escherichia coli controlled by the Cpx-signaling pathway. Proc Natl Acad Sci U S A. 2002;99(4):2287-92.

22. Nedal A, Raeder SB, Dalhus B, Helgesen E, Forstrom RJ, Lindland K, et al. Peptides containing the PCNA interacting motif APIM bind to the beta-clamp and inhibit bacterial growth and mutagenesis. Nucleic Acids Res. 2020;48(10):5540-54.
23. Price NL, Raivio TL. Characterization of the Cpx regulon in Escherichia coli strain MC4100. J Bacteriol. 2009;191(6):1798-815.
24. Hirota N, Matsuura S, Mochizuki N, Mutoh N, Imae Y. Use of lipophilic cation-permeable mutants for measurement of transmembrane electrical potential in metabolizing cells of Escherichia coli. J Bacteriol. 1981;148(2):399-405.
25. Suzuki T, Murakami T, Iino R, Suzuki J, Ono S, Shirakihara Y, et al. F0F1-ATPase/synthase is geared to the synthesis mode by conformational rearrangement of epsilon subunit in response to proton motive force and ADP/ATP balance. J Biol Chem. 2003;278(47):46840-6.
26. Jensen PR, Michelsen O. Carbon and energy metabolism of atp mutants of Escherichia coli. J Bacteriol. 1992;174(23):7635-41.
27. Ye JZ, Su YB, Lin XM, Lai SS, Li WX, Ali F, et al. Alanine Enhances Aminoglycosides-Induced ROS Production as Revealed by Proteomic Analysis. Front Microbiol. 2018;9:29.
28. Ebbensgaard A, Mordhorst H, Aarestrup FM, Hansen EB. The Role of Outer Membrane Proteins and Lipopolysaccharides for the Sensitivity of Escherichia coli to Antimicrobial Peptides. Front Microbiol. 2018;9:2153.
29. Futaki S, Nakase I. Cell-Surface Interactions on Arginine-Rich Cell-Penetrating Peptides Allow for Multiplex Modes of Internalization. Acc Chem Res. 2017;50(10):2449-56.
30. Hughes D, Andersson DI. Evolutionary Trajectories to Antibiotic Resistance. Annu Rev Microbiol. 2017;71:579-96.
31. Gerrish PJ, Lenski RE. The fate of competing beneficial mutations in an asexual population. Genetica. 1998;102-103(1-6):127-44.
32. Mechaly AE, Haouz A, Sassoon N, Buschiazzo A, Betton JM, Alzari PM. Conformational plasticity of the response regulator CpxR, a key player in Gammaproteobacteria virulence and drug-resistance. J Struct Biol. 2018;204(2):165-71.
33. Bryan LE, Kwan S. Roles of ribosomal binding, membrane potential, and electron transport in bacterial uptake of streptomycin and gentamicin. Antimicrob Agents Chemother. 1983;23(6):835-45.
34. Vanhoof R, Sonck P, Hannecart-Pokorni E. The role of lipopolysaccharide anionic binding sites in aminoglycoside uptake in Stenotrophomonas (Xanthomonas) maltophilia. J Antimicrob Chemother. 1995;35(1):167-71.
35. Gomez JE, Kaufmann-Malaga BB, Wivagg CN, Kim PB, Silvis MR, Renedo N, et al. Ribosomal mutations promote the evolution of antibiotic resistance in a multidrug environment. Elife. 2017;6.
36. Frimodt-Moller J, Rossi E, Haagensen JAJ, Falcone M, Molin S, Johansen HK. Mutations causing low level antibiotic resistance ensure bacterial survival in antibiotic-treated hosts. Sci Rep. 2018;8(1):12512.
37. El Meouche I, Dunlop MJ. Heterogeneity in efflux pump expression predisposes antibiotic-resistant cells to mutation. Science. 2018;362(6415):686-90.
38. Baba T, Ara T, Hasegawa M, Takai Y, Okumura Y, Baba M, et al. Construction of Escherichia coli K-12 in-frame, single-gene knockout mutants: the Keio collection. Mol Syst Biol. 2006;2:2006 0008.
39. Kitagawa M, Ara T, Arifuzzaman M, Ioka-Nakamichi T, Inamoto E, Toyonaga H, et al. Complete set of ORF clones of Escherichia coli ASKA library (a complete set of E. coli K-12 ORF archive): unique resources for biological research. DNA Res. 2005;12(5):291-9.
40. J M. Experiments in Molecular Genetics1972.

41. Datsenko KA, Wanner BL. One-step inactivation of chromosomal genes in Escherichia coli K-12 using PCR products. Proc Natl Acad Sci U S A. 2000;97(12):6640-5.
42. Li XT, Thomason LC, Sawitzke JA, Costantino N, Court DL. Positive and negative selection using the tetA-sacB cassette: recombineering and P1 transduction in Escherichia coli. Nucleic Acids Res. 2013;41(22):e204.
43. Hancock REW. MIC Determination By Microtitre Broth Dilution Method 1999 [Available from: http://cmdr.ubc.ca/bobh/method/mic-determination-by-microtitre-broth-dilution-method/.
44. Hosoi S, Mochizuki N, Hayashi S, Kasai M. Control of membrane potential by external H+ concentration in Bacillus subtilis as determined by an ion-selective electrode. Biochim Biophys Acta. 1980;600(3):844-52.
45. Liu X, Li Y, Guo Y, Zeng Z, Li B, Wood TK, et al. Physiological Function of Rac Prophage During Biofilm Formation and Regulation of Rac Excision in Escherichia coli K-12. Sci Rep. 2015;5:16074.
46. Keyhani NO, Bacia K, Roseman S. The transport/phosphorylation of N,N'-diacetylchitobiose in Escherichia coli. Characterization of phospho-IIB(Chb) and of a potential transition state analogue in the phosphotransfer reaction between the proteins IIA(Chb) AND IIB(Chb). J Biol Chem. 2000;275(42):33102-9.
47. Conter A, Menchon C, Gutierrez C. Role of DNA supercoiling and rpoS sigma factor in the osmotic and growth phase-dependent induction of the gene osmE of Escherichia coli K12. J Mol Biol. 1997;273(1):75-83.
48. Sukhodolets MV, Cabrera JE, Zhi H, Jin DJ. RapA, a bacterial homolog of SWI2/SNF2, stimulates RNA polymerase recycling in transcription. Genes Dev. 2001;15(24):3330-41.
49. Yethon JA, Heinrichs DE, Monteiro MA, Perry MB, Whitfield C. Involvement of waaY, waaQ, and waaP in the modification of Escherichia coli lipopolysaccharide and their role in the formation of a stable outer membrane. J Biol Chem. 1998;273(41):26310-6.
50. Ma Q, Yang Z, Pu M, Peti W, Wood TK. Engineering a novel c-di-GMP-binding protein for biofilm dispersal. Environ Microbiol. 2011;13(3):631-42.
51. Guyer MS, Reed RR, Steitz JA, Low KB. Identification of a sex-factor-affinity site in E. coli as gamma delta. Cold Spring Harb Symp Quant Biol. 1981;45 Pt 1:135-40.
52. Charbon G, Campion C, Chan SH, Bjorn L, Weimann A, da Silva LC, et al. Re-wiring of energy metabolism promotes viability during hyperreplication stress in E. coli. PLoS Genet. 2017;13(1):e1006590.

Acknowledgments

This paper is dedicated to the memory of Mads Christian Guldbæk (1991-2019). **Funding**: This research was funded by grants from the Danish National Research Foundation (DNRF120), the Novo Challenge Center for Peptide-Based Antibiotics (NNF16OC0021700), A.P. Møller Lægefonden, Augustinus Fonden, Aase og Ejnar Danielsens Fond, and Brødrene Hartmanns Fond, the program NTNU Health at Norwegian University of Science and Technology (NTNU), and Trond Mohn foundation, Norway. **Author contributions**: Conceptualization: JFM, PEN, and ALO; data curation: JFM and AK; formal analysis: JFM, AK, and ALO; investigation: JFM and AK; methodology: JFM, AK, GC, and ALO; project administration: JFM and ALO; resources: JFM, PEN, and ALO; bioinfomatics: GC; supervision: PEN and ALO; manuscript writing: JFM; manuscript

editing: JFM, AK, GC, MO, PEN, and ALO. **Competing interests**: The authors declare that they have no competing interests. **Data and materials availability**: All data needed to evaluate the conclusions in the paper are present in the paper and/or the Supplementary Materials. Additional data are available from authors upon request. All figures were created with BioRender.com.

Figures and Tables

Fig. 1. *cpxR$_{L20Q}$* and *cpxA$_{\Delta 16\text{-}17}$* activates the Cpx-response.

A schematic model of the Cpx, Rcs, Psp, Bae, and σ^E stress response to R-PNA in the cytoplasmic membrane. Here, R-PNA does not activate the Cpx-response; however, an activated Cpx-response is the only of the five-tested extracytoplasmic stress responses that diminish R-PNA activity. The green plus sign indicates a constitutive active ESR where an activated Cpx-response confers resistance to R-PNA. A and B: MIC determinations for CPP-PNA/APIM for wild-type and mutants in µM. MIC were determined using broth dilutions (see Methods) at 37°C (no shaking). Peptide-PNA sequences are listed in Table 1. pCA24n-based plasmids were induced with 0.1 mM IPTG. C: *cpxP* expression determined by RT-qPCR (see Methods). All values are indicated as fold change relative to wild-type (dashed line). Experiments were performed in triplicate. D: MIC determinations for activated extracytoplasmic stress response-systems in µM (see text for details). The five extracytoplasmic stress responses were individually activated by overproduction of *nlpE* for the Cpx-pathway, *baeR* for the Bae-pathway, *rcsB* for the Rcs-pathway, *pspF* for the Psp-pathway, and *rpoE* for the σ^E-pathway(10). A dashed line indicates the wild-type MIC. Peptide-PNA sequences are listed in Table 1. pCA24n-based plasmids were induced with 0.1 mM IPTG.

Fig 2. Cpx-mediated downregulation of NDH-I and cytochrome *bo$_3$* oxidase leads to a decreased $\Delta\Psi$ across the cytoplasmic membrane that confers resistance to CPP$_{R11}$-APIM, CPP$_{RXR}$-PNA, and aminoglycosides.

A schematic model of an activated Cpx-response (shown here with a green plus sign) that leads to downregulation of both *nuoA* (NDH-I) and *cyoA* (cytochrome *b*o$_3$ oxidase), which consequently results in a decreased $\Delta\Psi$ across the cytoplasmic membrane that confers cross resistance to CPP$_{RXR}$-PNA and aminoglycosides. A: *nuoA* and *cyoA* expression determined by RT-qPCR (see Methods). All values are indicated as fold change relative to wild-type (dashed line). Experiments were performed in biological triplicates. B and C: MIC values for CPP-PNA/APIM (in µM) and aminoglycosides (in µg/mL) for wild-type and mutants. MIC were determined using broth dilutions (see Methods) at 37°C (no shaking). Peptide-PNA sequences are listed in Table 1. D: $\Delta\Psi$ across the cytoplasmic membrane as measured by the TPP^+ uptake for wild-type, *cpxR$_{L20Q}$*, *cpxA$_{\Delta 16\text{-}17}$*, Δ*cyo*, and Δ*nuo*. Experiments were performed as a minimum in biological triplicates.

Fig. 3. The magnitude of $\Delta\Psi$ across the cytoplasmic membrane determines CPP$_{RXR}$-PNA and aminoglycoside tolerance.

A schematic model of PMF across the cytoplasmic membrane. pH_I is pretty constant over the growth pH_o range (5.5 to 8.5), but the contributions of $\Delta\Psi$ and ΔpH vary(9). A: MIC determinations for wild-type tested against CPP_{RXR}-PNA, CPP_{R11}-APIM, CPP_{KFF}-PNA and gentamicin anaerobically or at pH 6.0. CPP-PNA/APIM MICs are given in µM (left y-axes) and gentamicin MICs are given in µg/mL (right y-axes). Wild-type MIC are given for aerobic growth conditions at pH 7.2 identical to the growth conditions for the ALE-experiment. B: MIC determinations for wild-type tested against CPP_{RXR}-PNA, CPP_{R11}-APIM, CPP_{KFF}-PNA and gentamicin at pH 8.0, supplemented w. 100 mM alanine, or with either *atpA* or *atpB* deleted. Peptide-PNA MICs are given in µM (left y-axes) and gentamicin MICs are given in µg/mL (right y-axes). Wild-type MIC are given for aerobic growth conditions at pH 7.2 identical to the growth conditions for the ALE-experiment.

Fig. 4. CPP_{RXR}-PNA, CPP_{R11}-APIM, and aminoglycoside uptake wild-type (A) and *cpx (B).**

A schematic model of CPP_{RXR}-PNA, CPP_{R11}-APIM, and aminoglycoside (AG) internalization across the cytoplasmic membrane and action in wild-type (A) and a *cpx**mutant (B). A: In the wild-type CPP_{RXR}-PNA, CPP_{R11}-APIM, and AG crossing of the cytoplasmic membrane from the periplasmic space and into the cytosol correlates with the magnitude of the $\Delta\Psi$. The respiratory complexes NADH:ubiquinone oxidoreductase complex I (NDH-I) transcribed from the *nuoABCEFGHIJKLMN*-operon (*nuo*) and cytochrome bo_3 ubiquinol oxidase (Cyo) transcribed from the *cyoABCDE* operon (*cyo*) are shown. CPP_{RXR}-PNA, AG, and CPP_{R11}-APIM in the cytosol leads to growth arrest by steric hindrance of ribosome binding to *acpP* mRNA for CPP_{RXR}-PNA (A.a), binding to the 30S subunit of ribosomes impairing translational accuracy (A.b), and binding to the β-clamp, respectively. B: In a *cpx** mutant CPP_{RXR}-PNA, CPP_{R11}-APIM, and AG are not able to transvers the cytoplasmic membrane from the periplasmic space and into the cytosol. The constitutive active Cpx-response downregulates *nuo, cyo*, which results in a reduced $\Delta\Psi$, which correlates with reducing killing for all the compounds. Lack of CPP_{RXR}-PNA and AG in the cytosol leads to translation of *acpP* mRNA (B.a) wild-type like 30S ribosomal function (B.b), and wild-type like β-clamp function, respectively, both leading to survival during CPP_{RXR}-PNA, CPP_{R11}-APIM, and AG treatment.

Table 1. Minimum inhibitory concentration to peptide-PNA (in µM).

Compound[a]	CPP	Target gene /protein	Wild-type	R-PNA^R		
				Ahx^R-1	Ahx^R-2	Ahx^R-3
CPP_{RXR}-PNA(4)	Arginine-rich CPP_{RXR}[a]	*acpP*[d]	0.5	8	8	8
CPP_{RXR}-PNA_{mm}(4)		*acpP* mismatch[e]	>16	>16	>16	>16
CPP_{RXR}-PNA_{ftsZ}(4)		*ftsZ*[f]	0.5	8	8	8
CPP_{RXR}-PNA_{ftsZ_mm}(4)		*ftsZ* mismatch[g]	>16	>16	>16	>16
CPP_{R11}-APIM(22)	Arginine-rich CPP_{R11}[b]	β-clamp (DnaN)[h]	1	N/A	N/A	N/A
PP_{KFF}-PNA(4)	Lysine-phenylalanine CPP_{KFF}[c]	*acpP*[d]	0.25	0.25	0.25	0.25
CPP_{KFF}-PNA_{mm}(4)		*acpP* mismatch[f]	>16	>16	>16	>16

[a] [a] Arginine-rich CPP_{RXR}: H-(R-Ahx-R)$_4$-Ahx-(βAla). For the CPP-part amino acids are shown in uppercase letters. Ahx: 6-aminohexanoic acid;; [b] Arginine-rich CPP_{R11}: RRRRRRRRRRR; [c] Lysine-rich CPP_KFF: H-(KFF)$_3$K-eg1; [d] *acpP* target sequence (5'-3'): H-ctcatactct-NH_2; [e] *acpP* mismatch sequence (the two mismatch are underlined, 5'-3'): H-ctc<u>t</u>tac<u>a</u>ct-NH_2; [f] *ftsZ* target sequence (5'-3'): H-ttcaaacatagt-NH_2; [g] *ftsZ* mismatch sequence (the two mismatch are underlined, 5'-3'): [h] H-ttc<u>t</u>aaca<u>a</u>agt-NH_2; [i] Ac-MD-RWLVK-GILQWRKI (RWLVK*). MIC determinations for peptide-PNA are in µM. MIC were determined using broth dilutions (see Methods) at 37°C (no shaking).

Table 2. CPP_{RXR}-PNA resistant genotypes

					Evolved towards CPP_{RXR}-PNA		
				Linage[c]	#1		#2
Mutation type[a]				**Region/gene[b]**	Frequency[d]	2/5	3/5	5/5
IS	IN	DEL	SNP		Strain	**Ahx^R-1**	**Ahx^R-2**	**Ahx^R-3**
IS1				IG: *chbB - osmE*		x	x	
IS5				IG: *gltF - yhcA*		x	x	x
IS1				*rapA*		x	x	
IS1				*waaB*		x	x	x
IS1				*waaO*		x	x	x
			x	$yfaP_{V55G}$		x		
			x	$rpsL_{I82D}$		x	x	x
			x	$bdcA_{A53T}$		x		
			x	$cpxR_{L20Q}$				x
		x		*Δrac*			x	

Mutational profile of CPP_{RXR}-PNA^R clones. [a] Mutation type; IS: IS insertion; IN: insertion; DEL: deletion; SNP: single-nucleotide polymorphism. [b] Mutated genomic region; IG: inter genic region between two genes;

Δ*rac*; excerted *rac* prophage(45). [c] Indicates which lineage the evolved clones where isolated from within the ALE-experiment with CPP_{RXR}-PNA. [d] Frequency of the evolved clone within the lineage. See Table S1 for mutation details and Table S2 for function of the mutated genes.

Fig.1

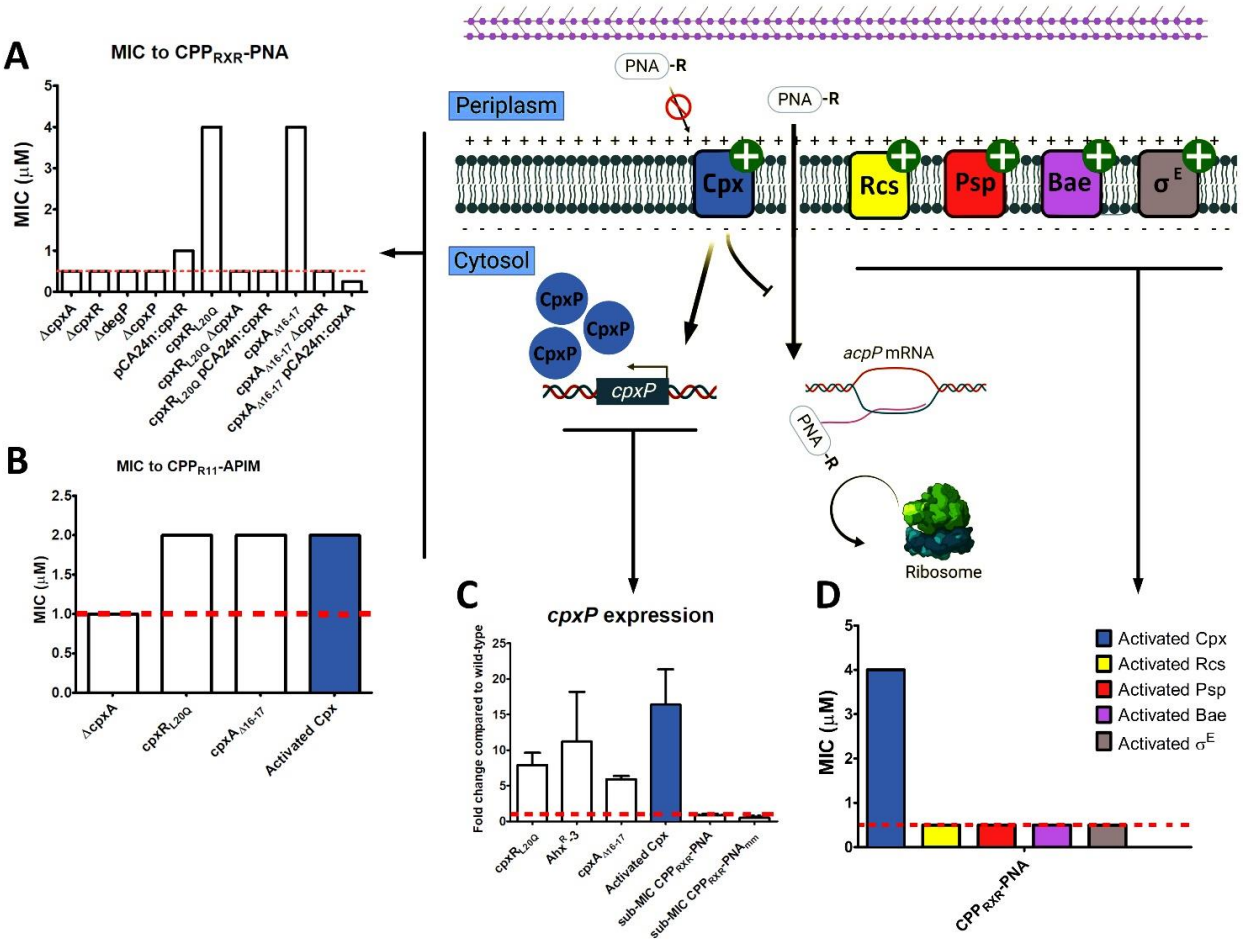
A
MIC to CPP$_{RXR}$-PNA
MIC (μM)
ΔcpxA
ΔcpxR
ΔdegP
ΔcpxP
pCA24n:cpxR
cpxR$_{L20Q}$
cpxR$_{L20Q}$ ΔcpxA
cpxR$_{L20Q}$ pCA24n:cpxR
cpxA$_{Δ16-17}$
cpxA$_{Δ16-17}$ ΔcpxR
cpxA$_{Δ16-17}$ pCA24n:cpxA
B
MIC to CPP$_{R11}$-APIM
MIC (μM)
ΔcpxA
cpxR$_{L20Q}$
cpxA$_{Δ16-17}$
Activated Cpx
Periplasm
Cytosol
PNA -R
PNA -R
Cpx
Rcs
Psp
Bae
σ^E
CpxP
CpxP
CpxP
cpxP
acpP mRNA
PNA -R
Ribosome
C
cpxP expression
Fold change compared to wild-type
cpxR$_{L20Q}$
Ahx^R-3
cpxA$_{Δ16-17}$
Activated Cpx
sub-MIC CPP$_{RXR}$-PNA
sub-MIC CPP$_{RXR}$-PNA$_{mm}$
D
MIC (μM)
Activated Cpx
Activated Rcs
Activated Psp
Activated Bae
Activated σ^E
CPP$_{RXR}$-PNA

Fig. 2

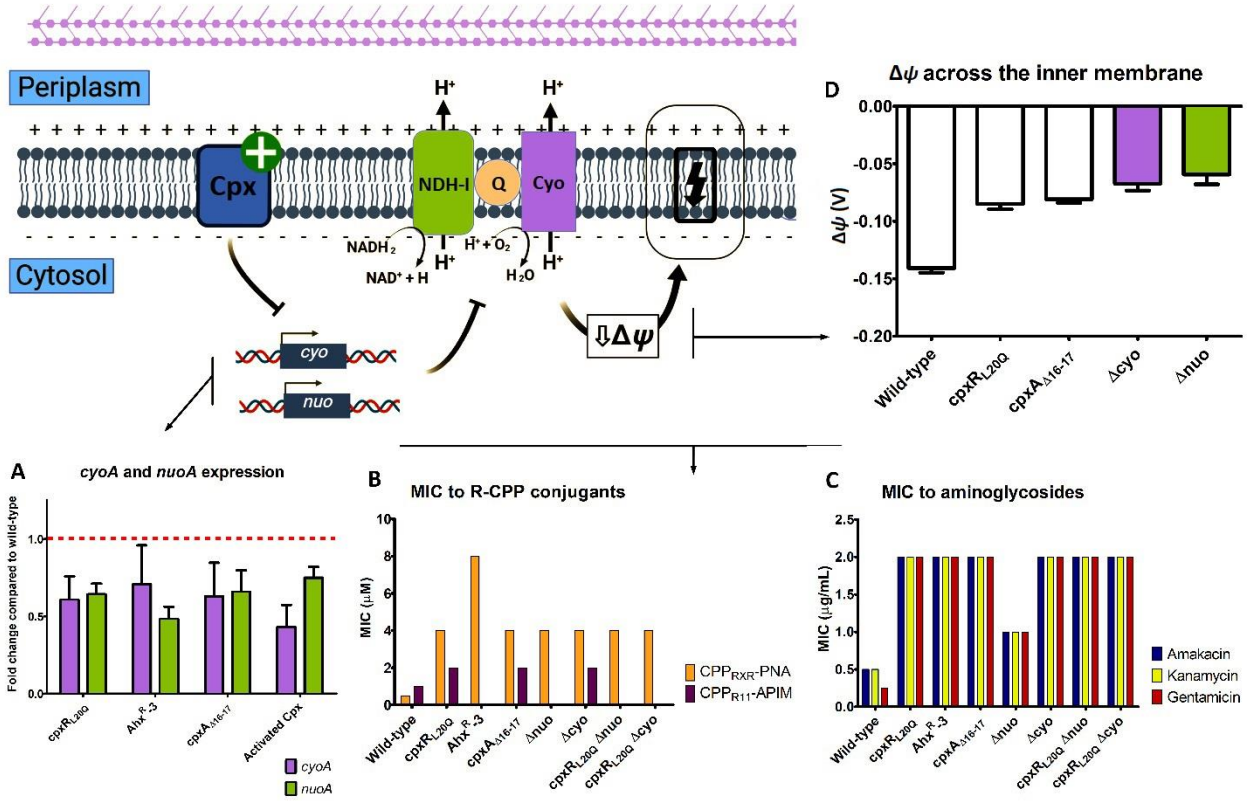
Periplasm
Cytosol
Cpx
NDH-I
Q
Cyo
H+
NADH2
NAD+ + H
H+ + O2
H2O
⇩Δψ
cyo
nuo
D
Δψ across the inner membrane
Δψ (V)
Wild-type
cpxRL20Q
cpxAΔ16-17
Δcyo
Δnuo
A
cyoA and nuoA expression
Fold change compared to wild-type
Activated Cpx
cyoA
nuoA
B
MIC to R-CPP conjugants
MIC (μM)
CPPRXR-PNA
CPPR11-APIM
C
MIC to aminoglycosides
MIC (μg/mL)
Amakacin
Kanamycin
Gentamicin

Fig. 3.

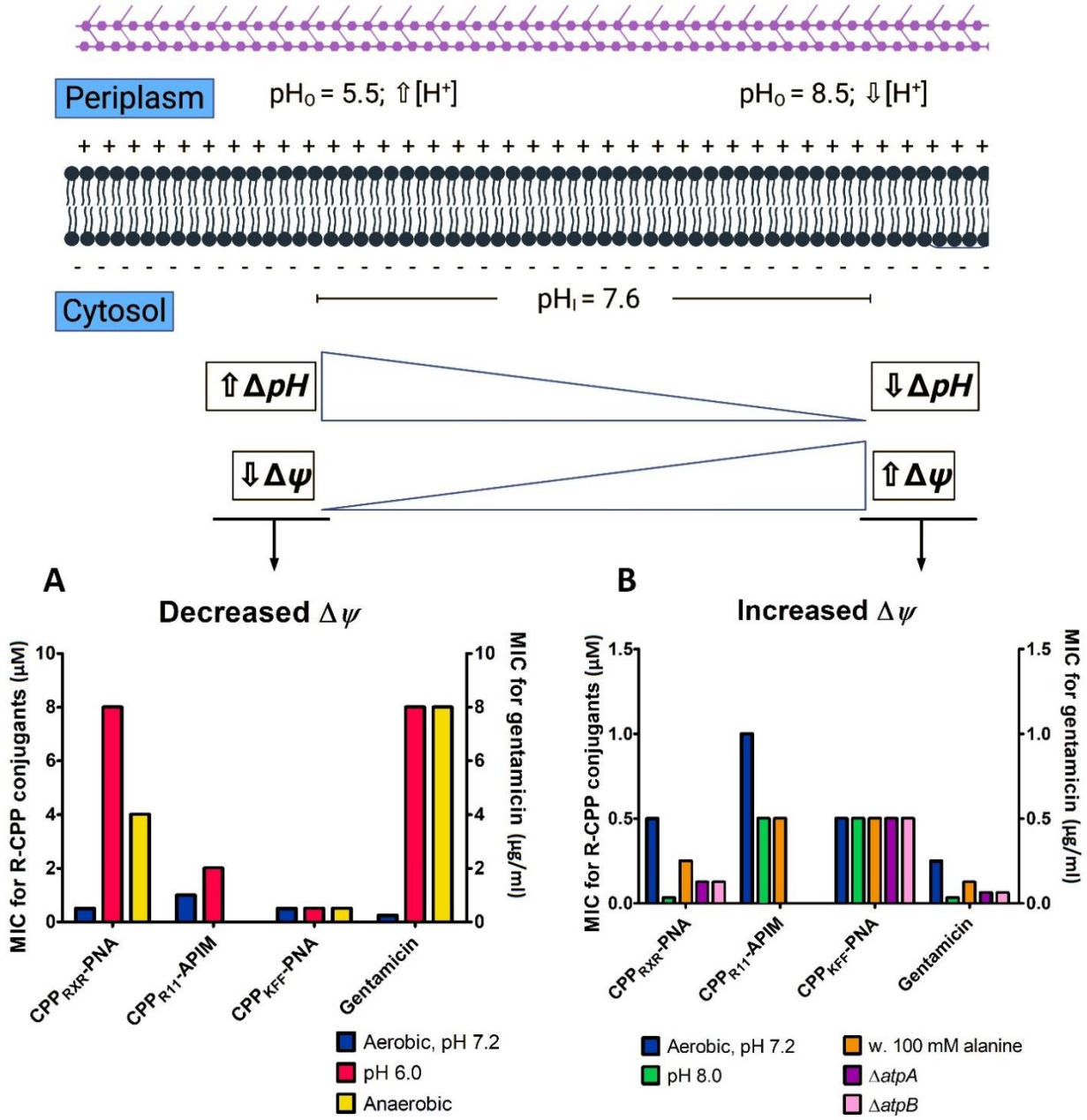
Periplasm
pH$_O$ = 5.5; ⇧[H$^+$]
pH$_O$ = 8.5; ⇩[H$^+$]
Cytosol
pH$_I$ = 7.6
⇧ΔpH
⇩ΔpH
⇩Δψ
⇧Δψ
A
Decreased Δψ
B
Increased Δψ
MIC for R-CPP conjugants (μM)
MIC for gentamicin (μg/ml)
CPP$_{RXR}$-PNA
CPP$_{R11}$-APIM
CPP$_{KFF}$-PNA
Gentamicin
Aerobic, pH 7.2
pH 6.0
Anaerobic
pH 8.0
w. 100 mM alanine
Δ*atpA*
Δ*atpB*

Fig. 4.

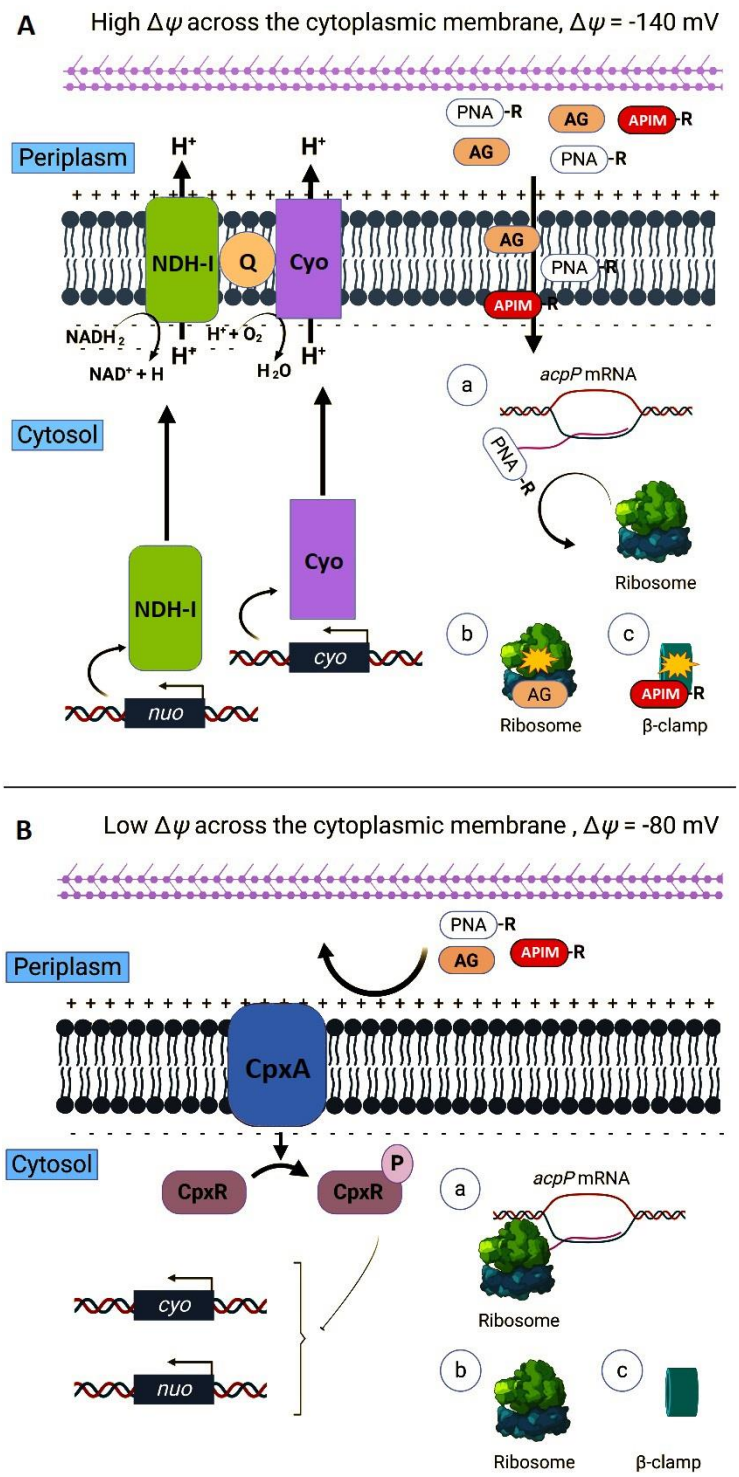
A
High Δψ across the cytoplasmic membrane, Δψ = -140 mV
Periplasm
Cytosol
NDH-I
Q
Cyo
NADH2
NAD+ + H
H+ + O2
H2O
H+
PNA -R
AG
APIM -R
acpP mRNA
Ribosome
β-clamp
nuo
cyo
a
b
c
B
Low Δψ across the cytoplasmic membrane , Δψ = -80 mV
CpxA
CpxR
P

Supplementary Materials

Table S1. Mutation type.

Gene	Start (bp)	Mutation type	Mutation	Change
IG: *chbB* - *osmE*	1821764	IS1 insertion		
IG: *gltF* - *yhcA*	3362023	IS5 insertion		
rapA	63248	IS1 insertion		
waaB	3803557	IS1 insertion		
waaO	3802515	IS1 insertion		
$yfaP_{V55G}$	2327980	SNP	A → G	Valine-55-Glycine
$rpsL_{I82D}$	3474308	SNP	A → T	Isoleucine-82-Asparagine
$bdcA_{A53T}$	4473895	SNP	C → T	Alanine-53-Threonine
$cpxR_{L20Q}$	4105612	SNP	A → T	Leucine-20-Glutamine
Δrac	1411941	Deletion	23 kb del	Excerted *rac* prophage(45)

Table S2. Function of mutated genes.

Gene	Function	Reference
chbB	*N,N'*-diacetylchitobiose-specific phosphotransferase system enzyme IIB component	(46)
osmE	Osmotically-inducible lipoprotein, which is induced at the onset of stationary phase	(47)
gltF	Unknown	(18)
yhcA	Hypothetical protein, function unknown	
rapA	RapA enables recycling of stalled RNA polymerases and stimulates RNA synthesis *in vitro*	(48)
waaB	The *waa*-operon consists of *waaQGPSBOJYZU* whose products are involved in the assembly of the core region of the lipopolysaccharide molecule in the outer membrane of the cell envelope.	(49)
waaO		
yfaP	Unknown	
rpsL	The product of *rpsL* is the S12 protein; a component of the 30S subunit of the ribosome that plays a role in translational accuracy.	(20)
bdcA	BdcA is a c-di-GMP-binding biofilm dispersal mediator protein	(50)
cpxA	*cpxAR* encodes the two-component regulatory system CpxA/R, that consists of the transmembrane sensor kinase CpxA in conjunction with the cytoplasmic transcription factor CpxR.	(21)
cpxR		

Table S3. Accumulated fitness gain mutations from the ALE-experiment to the media alone.

Gene	Start (bp)	Mutation type	Mutation	Change
yiaD	3716565	SNP	C → T	Leucine-7-Phenylalanine
uspC	1979381	IS1 insertion		
uspC	1979385	IS1 insertion		
uspC	1979486	IS1 insertion		
uspC	1979489	IS1 insertion		
uspC	1979507	IS1 insertion		
uspC	1979510	IS1 insertion		
ccmA	2297378	IS1 insertion		
ccmA	2297389	IS1 insertion		
fimE	4542161	Inversion/duplication		
fimE	4542164	Inversion/duplication		
fimE	4542682	Inversion/duplication		
fimE	4542689	Inversion/duplication		
fimE	4542690	Inversion/duplication		
fimE	4542987	Inversion/duplication		
fimE	4542995	Inversion/duplication		

Table S4. ***cpxR$_{L20Q}$ and cpxA$_{\Delta 16\text{-}17}$ does not provide tolerance to cationic antimicrobial peptides.***

Minimum inhibitory concentration to peptide-PNA/APIM (in µM) and AMPs (in µg/mL)					
AMP/strain	**Wild-type**	***cpxA$_{\Delta 16\text{-}17}$***	***cpxR$_{L20Q}$***	**Δ*waaBO***	**Ahx^{R}-3**
CPP$_{RXR}$-PNA	0.5	4	4	0.5	8
CPP$_{R11}$-APIM	1	2	2	1	N/A
Cecropin P1	32	32	32	16	16
Cap11	2	2	2	1	1
Cap18	2	2	2	1	1
Indolicidin	4	4	4	4	4
Apidaecin 1B	8	8	8	8	8
Colistin	0.125	0.125	0.125	0.0625	0.0625
Protamine	16	16	16	16	16

Table S4. MIC values for peptide-PNA (in µM) and AMPs (in µg/mL) for wild-type and indicated mutants. MIC were determined using broth dilutions (see Methods) at 37°C (no shaking). Peptide-PNA sequences are listed in Table 1.

Table S5. Bacterial strains.

Strain	Genotype	Abbreviated form	Reference/source
MG1655	$F^-\lambda^-$*rph-1*	Wild-type	(51)
ALO6524	Δ*cpxA*:kan[a]	Δ*cpxA*	This work
ALO6525	Δ*cpxR*:kan[a]	Δ*cpxR*	This work
ALO7548	Δ*degP*:kan[a]	Δ*degP*	This work
ALO7549	Δ*cpxP*:kan[a]	Δ*cpxP*	This work
ALO4576	Δ*atpA*:cat[a]	Δ*atpA*	(52)
ALO4577	Δ*atpB*:cat[a]	Δ*atpB*	(52)
ALO7180	$cpxR_{L20Q}$[a]	$cpxR_{L20Q}$	This work
ALO7550	$cpxR_{L20Q}$ Δ*cpxA*:kan[a]	$cpxR_{L20Q}$ Δ*cpxA*	This work
ALO7552	$cpxR_{L20Q}$ Δ*nuoABCEFGHIJKLMN*:cat[a]	$cpxR_{L20Q}$ Δ*nuo*	This work
ALO7553	$cpxR_{L20Q}$ Δ*cyoABCDE*:cat[a]	$cpxR_{L20Q}$ Δ*cyo*	This work
ALO7554	$cpxA_{\Delta 16\text{-}17}$[a]	$cpxA_{\Delta 16\text{-}17}$	This work
ALO7551	$cpxA_{\Delta 16\text{-}17}$ Δ*cpxR*:kan[a]	$cpxA_{\Delta 16\text{-}17}$ Δ*cpxR*	This work
ALO7555	Δ*nuoABCEFGHIJKLMN*:cat[a]	Δ*nuo*	This work
ALO7556	Δ*cyoABCDE*:cat[a]	Δ*cyo*	This work
ALO6972	Δ*waaBO*:cat[a]	Δ*waaBO*	This work

[a] Genotype otherwise as *E. coli* MG1655

Table S6. Primer sequences.

Primers for cloning	
Primer	**Sequence**
*nuo*_cat_Fw	ccgccgagcatgtcggcggctttctgacttacaaagtaacagagtgtaggctggagctgcttc
*nuo*_cat_Rv	catctgccgtgaagagcagtgaatctggcgctacttttgatgagtaagcacatatgaatatcctccttag
*cyo*_cat_Fw	gctaagaaaaaaggtgccgtagcaccttttttaatagagaggttttggtgtaggctggagctgcttc
*cyo*_cat_Rv	tgcccacacactttaaacgccaccagatcccgtggaattgaggtcgttaacatatgaatatcctccttag
*waaB*_cat_Fw	ggaaatgagtccacaatgctacccttatatcattactttatagtttcccagttgtgtaggctggagctgcttc
*waaO*_cat_Rv	gacaaataaaaccgttaaaacagtgagttttactcaattaatgagagtttctcatatgaatatcctccttag
CpxR_*tet-sacB*_Fw	ggcgaagatgcgcgcggttaagctgcctatcatgaagcagaaaccatcagatcaaagggaaaactgtccatat
CpxR_*tet-sacB*_Rv	ttagcgacgtctgatgacgtaatttctgcctcggaggtatttaaacaatgtcctaatttttgttgacactcta
$CpxR_{L20Q}$_Fw	tgaatcgagcttgggtaaca
$CpxR_{L20Q}$_Rv	ggatggtgtctatggcaagg
Primers for qPCR	
Primer	**Sequence**
*cpxP*_qPCR_Fw	ggcatccgggtgaagaactt
*cpxP*_qPCR_Rv	aacttatgccgtcgaacatatgg
*nuoA*_qPCR_Fw	caccagataaaccagacctgcc
*nuoA*_qPCR_Rv	atctgttcgcatggtcaacctc
*cyoA*_qPCR_Fw	gactgcttcgcttttgcgac
*cyoA*_qPCR_Rv	aacgaacccggcacttatgac
*hctA*_qPCR_Fw	gcttttgccacgtattcgcc
*hctA*_qPCR_Rv	acttctctttgctgtcgccttc
*cysG*_qPCR_Fw	cgtcgattattgaccgctcacc
*cysG*_qPCR_Rv	cgaactgttgtttcactcgccc